PROCEEDINGS OF THE INTERNATIONAL WORKSHOP "FUSION DYNAMICS AT THE EXTREMES" - DUBNA-FLNR-RUSSIE 25-27 MAI 2000

G. ROYER AND R.A. GHERGHESCU

Rapport Interne SUBATECH 00-23

FUSION AND ALPHA EMISSION WITHIN A LIQUID DROP MODEL AND HEAVIEST ELEMENT FORMATION AND DECAY

G. ROYER
Laboratoire Subatech, 4 rue A. Kastler, 44072 Nantes Cedex 03, France
E-mail : royer@subatech.in2p3.fr

R. A. GHERGHESCU
National Institute for Physics and Nuclear Engineering,
P. O. Box MG-6, RO-76900 Bucharest, Romania

The potential energy governing the fusion and α emission processes has been determined within a generalized liquid drop model including the proximity effects, the asymmetry, an accurate nuclear radius and an adjustment to reproduce the experimental Q value. The α decay half-lives deduced from the WKB barrier penetration probability without adjustable preformation factor are in agreement with the experimental data in the whole mass range. Accurate simple formulas are proposed for $\log_{10}\left[T_{1/2;\alpha}(s)\right]$. Fusion barriers leading to the heaviest and superheavy elements as well as their α emission half-lives are presented and compared with recent experimental data.

1 Introduction

The synthesis of very heavy nuclides has apparently strongly progressed recently [1-3]. The observed decay mode is the α emission. The purpose of this work is to study the fusion barriers investigated in the recent experiments and to look at the α decay half-lives of the heaviest systems. Before, it will be checked that the α decay may be viewed as a very asymmetric fission [4] within the generalized liquid drop model (GLDM) which has allowed to reproduce most of the fusion and fission characteristics [5-7] and light nucleus emission [8].

2 Generalized Liquid Drop Model

The GLDM [5] includes an accurate nuclear radius, the mass and charge asymmetries and a proximity energy . This last term takes into account the effects of the surface tension forces between surfaces in regard in a neck or a gap. No frozen density approximation is done and the proximity function is effectively integrated in the neck and, consequently, the proximity energy depends on the nuclear shape and vanishes for no-necked nuclear configurations. The selected quasi-molecular shapes describe the rapid formation of a deep neck and its filling while keeping almost spherical ends (see Fig. 1).

This GLDM has allowed to reproduce accurately the empirical fusion barrier positions R_b and heights E_b . A recent fitting procedure has led to the following formulas : $R_b = \left(A_1^{1/3} + A_2^{1/3}\right)\left(1.908 - 0.0857\ln(Z_1Z_2) + 3.94/Z_1Z_2\right)$

$$E_b = -19.38 + \frac{2.1388Z_1Z_2 + 59.427\left(A_1^{1/3} + A_2^{1/3}\right) - 27.07\ln\left(\dfrac{Z_1Z_2}{A_1^{1/3} + A_2^{1/3}}\right)}{\left(A_1^{1/3} + A_2^{1/3}\right)\left(2.97 - 0.12\ln(Z_1Z_2)\right)}.$$

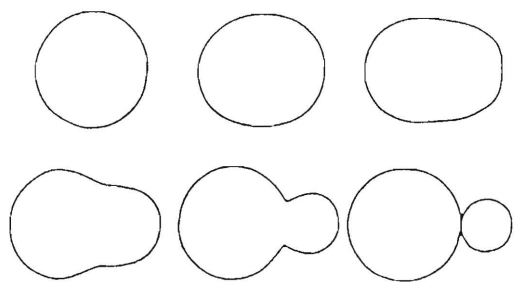

Fig. 1. Asymmetric shape sequence leading rapidly from a sphere to two tangent spheres assuming volume conservation.

3 Alpha decay

After the contact point the energy relatively to infinity is simply the sum of the Coulomb energy and the proximity energy reproduced by (see Fig. 2)

$$\frac{E_{prox}(\text{MeV})}{4\pi\gamma} = e^{-1.38(r - R_{cont})}\begin{bmatrix} 0.6584A^{2/3} - \left(\dfrac{0.172}{A^{1/3}} + 0.4692A^{1/3}\right)r \\ -0.02548A^{1/3}r^2 + 0.01762r^3 \end{bmatrix}$$

where A is the mass of the mother nucleus and r the distance between mass centres [9].

The difference between the experimental and theoretical Q_α values has been added at the sphere energy with a linear attenuation factor vanishing at the contact point [4]. The inadequacy of the pure Coulomb barrier is clearly displayed in Fig. 3. The proximity energy lowers the barrier height by several MeV and moves the top towards two separated fragments maintained in unstable equilibrium by the balance between the repulsive Coulomb forces and the attractive nuclear proximity forces.

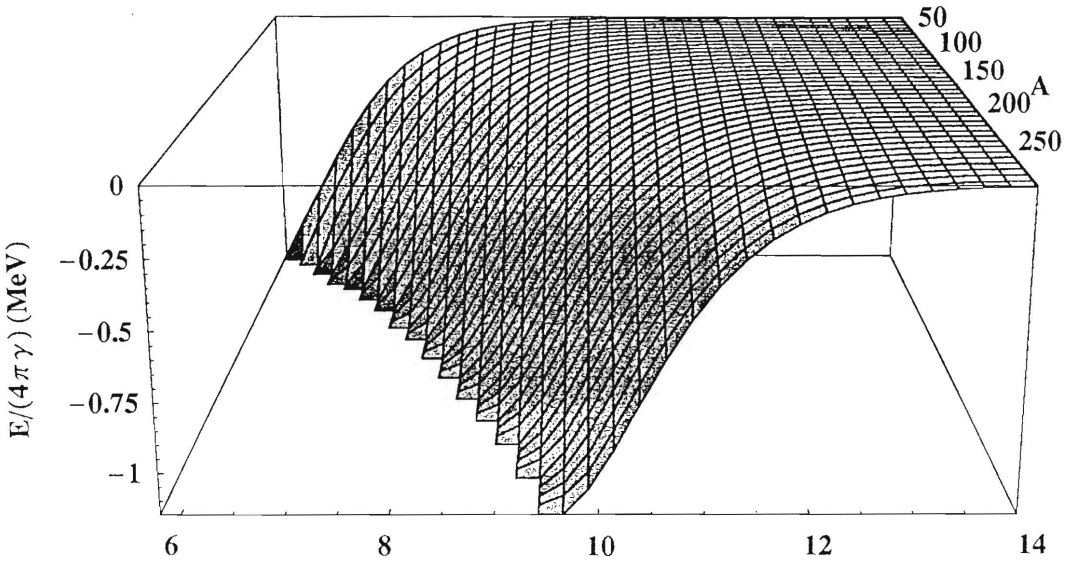

Fig. 2. Proximity energy $(/4\pi\gamma)$ between two separated α particle and daughter spherical nucleus A-4 as a function of the distance between the mass centres.

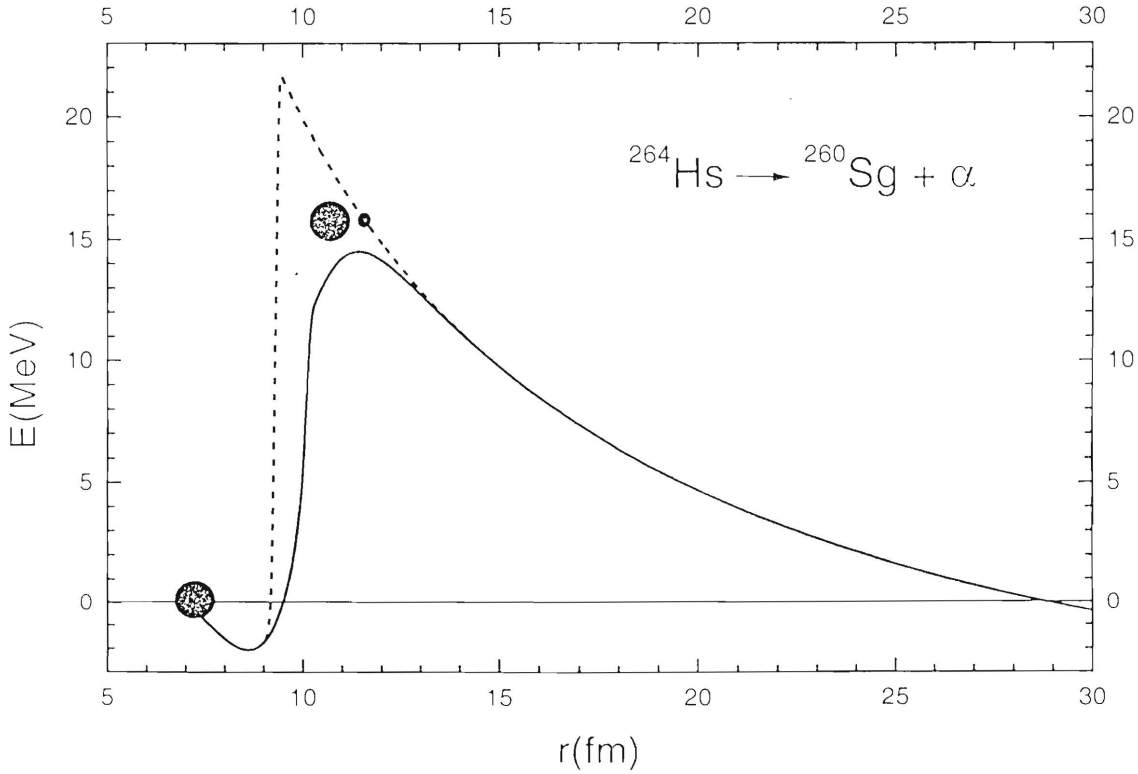

Fig. 3. α decay barrier for ^{264}Hs. The solid and dashed curves correspond to the barrier with and without a nuclear proximity energy term.

In such an unified fission model, the decay constant of the parent nucleus is simply defined as $\lambda = \nu_0 P$. There is no preformation probability factor. The assault frequency ν_0 has been chosen as $\nu_0 = 1.0 \times 10^{20} s^{-1}$. The barrier penetrability P is calculated within the general form of the action integral

$$P = \exp\left\{-\frac{2}{\hbar}\int_{R_{int}}^{R_{out}} \sqrt{2\mu[E(r) - E(R_{int})]}dr\right\} \text{ with } E(R_{int}) = E(R_{out}) = Q_{Exp}.$$

The ability to reproduce the experimental half-lives is shown in Fig. 4. The α decay half-lives of 373 nuclei have also been determined [4]. The rms deviation between the theoretical and experimental values of $\log_{10}[T_{1/2}(s)]$ is only 0.63.

In addition to the GLDM approach, a fitting procedure from the experimental data leads to the following formula for the 373 nuclei with a rms deviation of 0.42.

$$\log_{10}[T_{1/2}(s)] = -26.06 - 1.114A^{1/6}\sqrt{Z} + \frac{1.5837Z}{\sqrt{Q_\alpha}}.$$

For the subset of the 131 even-even nuclei the rms deviation between the theoretical and experimental values is only 0.35. Within the following formula the rms is 0.285.

$$\log_{10}[T_{1/2}(s)] = -25.31 - 1.1629A^{1/6}\sqrt{Z} + \frac{1.5864Z}{\sqrt{Q_\alpha}}.$$

For the subset of the 106 even-odd nuclei the rms deviation is 0.71. Within the following formula the rms is 0.39.

$$\log_{10}[T_{1/2}(s)] = -26.65 - 1.0859A^{1/6}\sqrt{Z} + \frac{1.5848Z}{\sqrt{Q_\alpha}}.$$

For the subset of the 86 odd-even nuclei the rms deviation is 0.57. The following formula leads to a rms of 0.36.

$$\log_{10}[T_{1/2}(s)] = -25.68 - 1.1423A^{1/6}\sqrt{Z} + \frac{1.592Z}{\sqrt{Q_\alpha}}.$$

For the subset of the 50 odd-odd nuclei the rms deviation is 0.99. The following formula leads to a rms of 0.35.

$$\log_{10}[T_{1/2}(s)] = -29.48 - 1.113A^{1/6}\sqrt{Z} + \frac{1.6971Z}{\sqrt{Q_\alpha}}.$$

4 On the heaviest and superheavy nuclides

In the fusion reactions leading to the heaviest elements the formation of the nucleon shells plays a main role to stabilize the system. The shell effects given by the asymmetric two center shell model have been added at the macroscopic GLDM [10] as well as the corrections to obtain the experimental Q value.

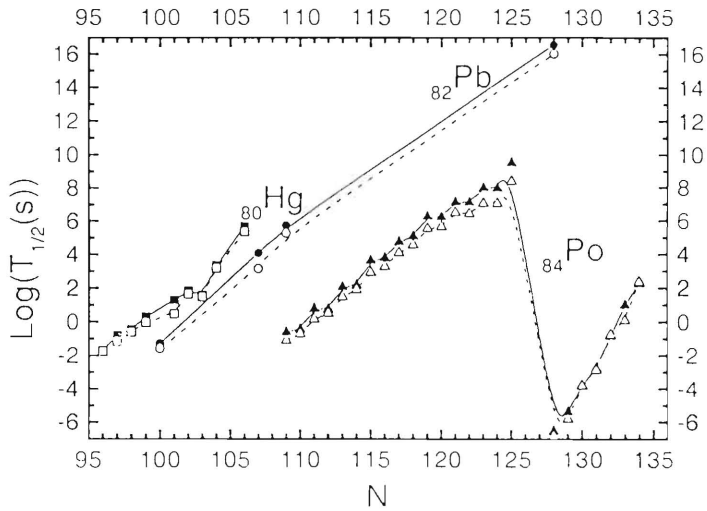

Fig. 4. $\log_{10}\left[T_{\alpha,1/2}(s)\right]$ for Hg, Pb and Po. The solid shapes and lines correspond to experimental data and the open shapes and dashed lines to the theoretical ones.

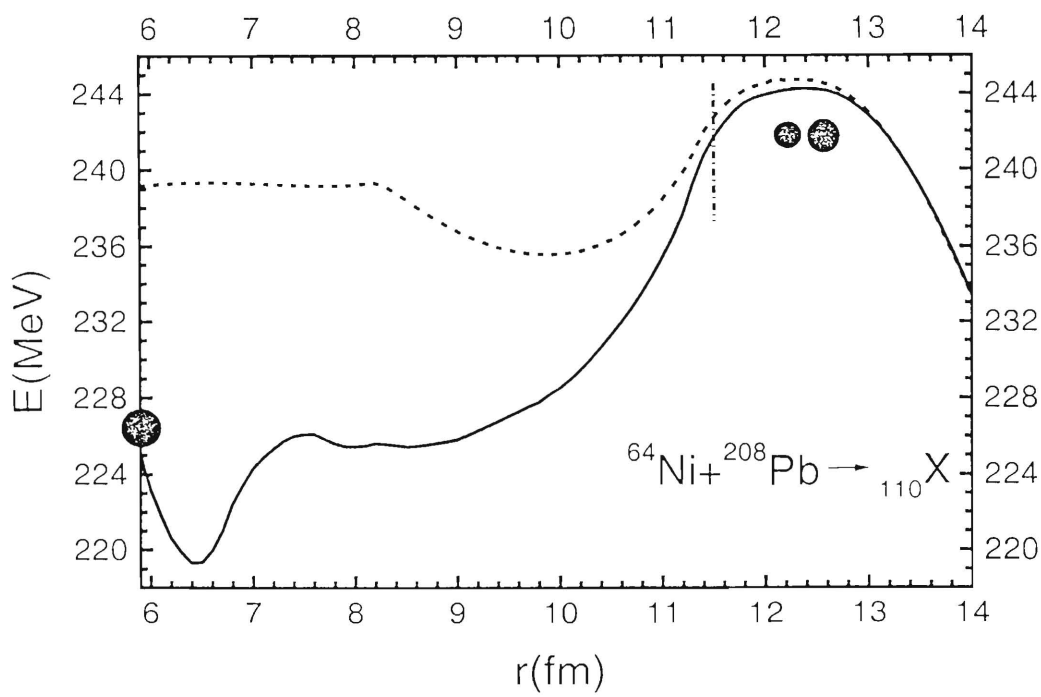

Fig. 5. Macroscopic (dashed curve) and microscopic (solid one) fusion barriers versus the mass-centre distance. The vertical line gives the contact point.

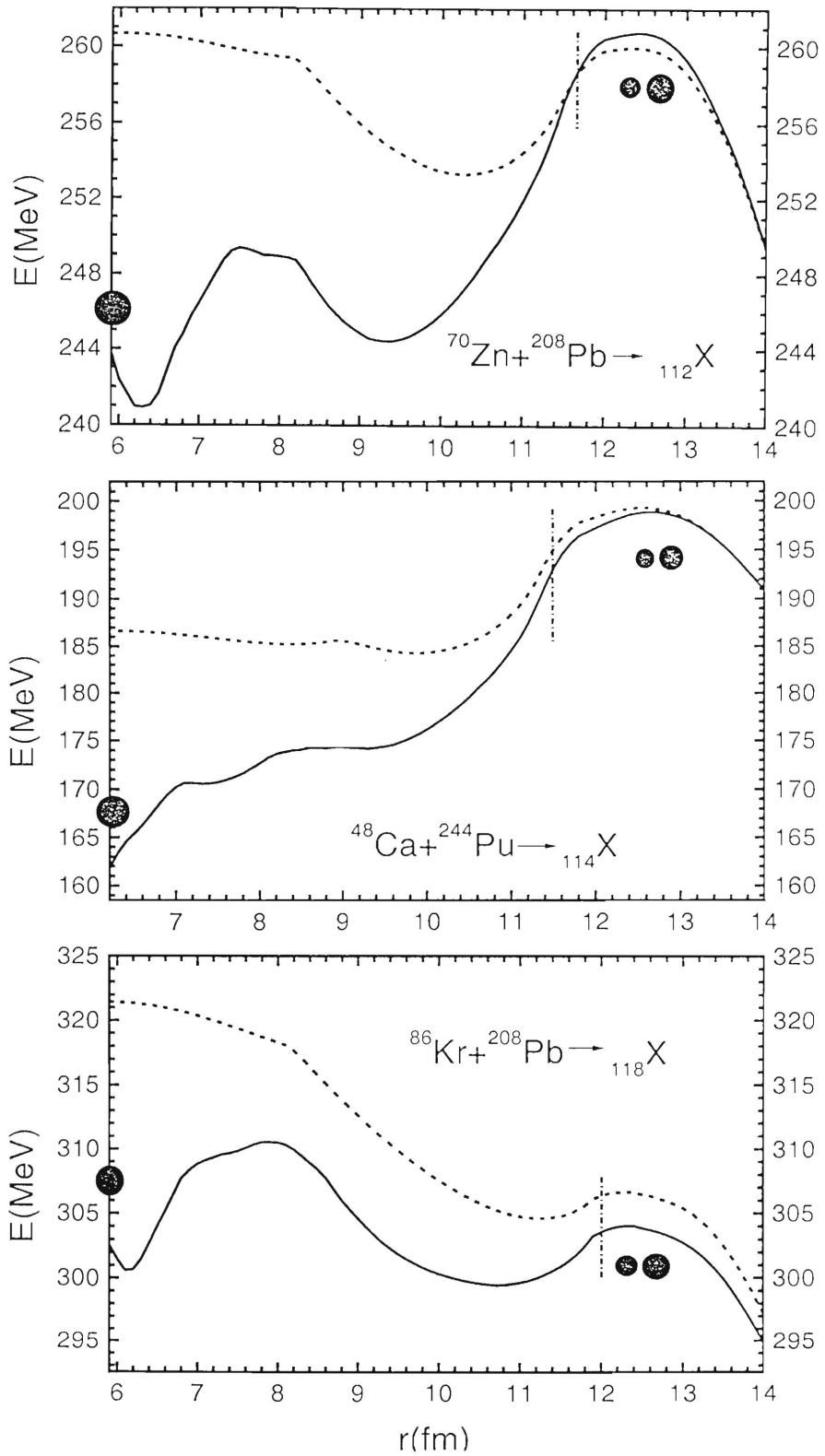
E(MeV)
$^{70}Zn+^{208}Pb \rightarrow {}_{112}X$
$^{48}Ca+^{244}Pu \rightarrow {}_{114}X$
$^{86}Kr+^{208}Pb \rightarrow {}_{118}X$
r(fm)

Macroscopically, a relative minimum appears at large deformations (see Fig. 5). Microscopically, for Ni + Pb the ground state is slightly deformed while a plateau lies at intermediate deformations. For Zn + Pb double humped barriers appear separated by a deep minimum and fast fission becomes an important decay channel. The moment of the neutron emission is decisive to decide between complete fusion and fast fission. For Ca + Pu, due the system asymmetry, the barrier against reseparation is high and the system will descend till the sphere configuration. The final excitation energy depends also strongly on the moment of emission of the three neutrons. For the Kr + Pb reaction, the inner barrier is the highest but a minimum still occurs near the sphere. The stability of such formed nuclear systems is another problem.

The characteristics of these fusion barriers are shown in table 1. Within the GLDM, the saddle-point corresponds always to two separated sphere configurations. The often used approximation which starts the fusion process from the contact point seems rough. At the contact point the first external peak of the fusion barrier is already passed. Macroscopically, the energy of the minimum at large deformations is lower than the sphere energy.

The barrier height derived from the GLDM is systematically higher than the Bass barrier [11] and the fusion radius is lower. These two effects lead to smaller fusion cross sections within the GLDM than within the Bass model. Indeed, for most of the incident energies presently used, the reaction is a subbarrier fusion for the GLDM while it is a fusion above the barrier for the Bass model. For the Kr + Pb, the incident energy is high (321 MeV in the mass centre) and leads to a reaction well above the barrier in the two models.

The predicted α decay half-lives of the heaviest elements have been calculated (see table 2) from the theoretical Q_α values given by the Thomas-Fermi model [12] since it reproduces nicely the mass decrements from Fermium to Z = 112. The values given by the GLDM should give a lower limit of the true value while the ones given by the fitted formulas should not be far from the reality. If such nuclei exist, their half-lives vary from microseconds to some days. Generally, for a given element, the half-lives increase with the neutron number.

The predictions of the GLDM agree (see table 3) with the apparently observed experimental data on the heaviest and superheavy isotopes except for three nuclei $^{285}114$ and $^{289}114$ and at a less degree $^{281}112$. The theoretical values are respectively of 5 to 2 orders of magnitude higher than the experimental data. One possible explanation of this discrepancy is perhaps that Z = 114 is not a good magic number as some studies using Hartree-Fock theory suggest and that the Thomas-Fermi model underestimates the Q_α value and, then, overestimates the half-lives. The analysis of the experimental data is also discussed [13]. With the GLDM, one obtains a kinetic energy of the fragments of 240 MeV, higher than the 190 MeV apparently measured. This is independent of the magicity of the charge number.

Reaction	Experimental result	R_{min} (fm)	H_{min} (MeV)	R_{ext} (fm)	H_{ext} (MeV)	H_{fus} (MeV)	E_{cm} (MeV)	R_{bass} (fm)	H_{bass} (MeV)
${}^{90}_{38}Sr+{}^{214}_{82}Pb$	? ${}^{304}_{120}X^*$	11.3	-15.0	12.2	-12.2	322.0	-	13.3	312.4
${}^{86}_{36}Kr+{}^{208}_{82}Pb$	${}^{293}_{118}Sh + 1n$	11.3	-16.8	12.0	-14.1	307.3	321	13.1	298.8
${}^{48}_{20}Ca+{}^{248}_{96}Cm$	? ${}^{296}_{116}X^*$	10.0	-3.5	12.6	11.2	203.1	-	13.0	198.5
${}^{82}_{34}Se+{}^{208}_{82}Pb$	? ${}^{290}_{116}X^*$	11.0	-14.5	11.9	-11.1	290.8	-	13.1	283.2
${}^{48}_{20}Ca+{}^{244}_{94}Pu$	${}^{289}_{114}Sh + 3n$	9.8	-2.4	12.6	12.6	199.3	197	13.0	194.8
${}^{48}_{20}Ca+{}^{242}_{94}Pu$	${}^{287}_{114}Sh + 3n$	9.9	-3.0	12.5	11.8	199.6	196	12.9	195.1
${}^{76}_{32}Ge+{}^{208}_{82}Pb$	? ${}^{284}_{114}X^*$	10.6	-11.0	11.8	-6.2	275.4	-	13.0	268.7
${}^{48}_{20}Ca+{}^{238}_{92}U$	${}^{283}_{112}Sh + 3n$	9.8	-1.9	12.5	13.3	195.8	192	12.9	191.4
${}^{70}_{30}Zn+{}^{208}_{82}Pb$	${}^{277}_{112}Sh + 1n$	10.3	-7.4	12.35	-0.7	260.0	257	12.9	254.1
${}^{64}_{28}Ni+{}^{209}_{83}Bi$	${}^{272}_{111}Sh + 1n$	10.0	-5.0	12.3	3.6	247.6	244	12.8	242.3
${}^{34}_{16}S+{}^{244}_{94}Pu$	${}^{273}_{110}Sh + 5n$	-	-	12.2	32.8	164.4	167	12.5	161.1
${}^{64}_{28}Ni+{}^{208}_{82}Pb$	${}^{271}_{110}Sh + 1n$	9.9	-3.6	12.3	5.5	244.7	239	12.8	239.4
${}^{62}_{28}Ni+{}^{208}_{82}Pb$	${}^{269}_{110}Sh + 1n$	9.6	-0.6	12.2	10.1	245.9	240	12.7	240.7
${}^{59}_{27}Co+{}^{209}_{83}Bi$	${}^{267}_{110}Sh + 1n$	9.5	0.1	12.2	11.7	241.1	235	12.7	236.1
${}^{58}_{26}Fe+{}^{209}_{83}Bi$	${}^{266}_{109}Mt + 1n$	9.6	-1.1	12.3	10.4	232.1	234	12.7	227.3

Table 1 Characteristics of the macroscopic fusion barriers leading to the heaviest nuclides. R_{min}, H_{min}, R_{ext} and H_{ext} are respectively the positions and energies relatively to the sphere of the external minimum and of the external peak of the fusion barrier. H_{fus} is the barrier height of the GLDM while R_{Bass} and H_{Bass} are the barrier radius and height given by the Bass model. E_{cm} is the centre of mass energy already used in an experiment.

	A	**286**	**287**	**288**	**289**	**290**	**291**	**292**	**293**	**294**	**295**	**296**	**297**	**298**	**299**
Z=118	**Qα**	13.27	13.11	13.11	12.99	13.04	12.79	12.59	12.49	12.51	12.42	12.52	12.34	12.73	12.87
	gldm	-6.87	-6.61	-6.63	-6.42	-6.52	-6.06	-5.69	-5.56	-5.60	-5.45	-5.66	-5.32	-6.11	-6.37
	fit	-6.35	-5.30	-6.07	-5.09	-5.97	-4.73	-5.09	-4.14	-4.96	-4.02	-5.02	-3.88	-5.49	-5.03
	A	**284**	**285**	**286**	**287**	**288**	**289**	**290**	**291**	**292**	**293**	**294**	**295**	**296**	**297**
Z=117	**Qα**	12.64	12.52	12.40	12.31	12.25	12.20	12.14	11.94	11.93	11.91	11.90	11.80	11.59	11.97
	gldm	-5.96	-5.74	-5.51	-5.36	-5.25	-5.16	-5.05	-4.64	-4.62	-4.64	-4.62	-4.43	-3.98	-4.83
	fit	-4.50	-4.74	-3.99	-4.33	-3.69	-4.12	-3.47	-3.58	-3.00	-3.55	-2.96	-3.34	-2.23	-3.76
	A	**281**	**282**	**283**	**284**	**285**	**286**	**287**	**288**	**289**	**290**	**291**	**292**	**293**	**294**
Z=116	**Qα**	12.39	11.90	12.03	11.83	11.68	11.65	11.52	11.55	11.50	11.34	11.33	11.03	11.15	11.19
	gldm	-5.67	-4.72	-5.01	-4.59	-4.27	-4.22	-3.96	-4.04	-3.94	-3.58	-3.57	-2.85	-3.19	-3.30
	fit	-4.35	-4.04	-3.61	-3.92	-2.86	-3.54	-2.52	-3.35	-2.51	-2.89	-2.14	-2.16	-1.74	-2.60
	A	**279**	**280**	**281**	**282**	**283**	**284**	**285**	**286**	**287**	**288**	**289**	**290**	**291**	**292**
Z=115	**Qα**	12.50	12.24	11.80	11.02	10.30	10.56	10.55	10.45	10.48	10.34	10.24	10.15	9.88	9.75
	gldm	-6.14	-5.65	-4.74	-3.01	-1.13	-1.85	-1.83	-1.58	-1.68	-1.32	-1.05	-0.80	-0.03	0.35
	fit	-5.21	-4.22	-3.73	-1.25	-0.02	-0.02	-0.74	0.26	-0.59	0.54	0.03	1.07	1.03	2.28
	A	**276**	**277**	**278**	**279**	**280**	**281**	**282**	**283**	**284**	**285**	**286**	**287**	**288**	**289**
Z=114	**Qα**	12.55	12.55	12.86	12.27	11.83	11.15	10.22	9.79	9.64	9.55	9.61	9.53	9.39	9.08
	gldm	-6.47	-6.48	-7.05	-5.97	-5.09	-3.58	-1.22	0.00	0.44	0.71	0.51	0.74	1.16	2.16
	fit	-5.94	-5.25	-6.60	-4.71	-4.49	-2.22	-0.54	1.38	1.10	2.07	1.16	2.10	1.80	3.49
	A	**274**	**275**	**276**	**277**	**278**	**279**	**280**	**281**	**282**	**283**	**284**	**285**	**286**	**287**
Z=113	**Qα**	12.20	12.12	12.11	12.37	12.77	12.83-	11.67	10.90	10.00	9.56	9.36	9.18	9.10	9.04
	gldm	-6.05	-5.90	-5.89	-6.41	-7.15	7.29	-5.05	-3.29	-0.93	0.35	0.96	1.53	1.78	1.96
	fit	-4.73	-4.97	-4.56	-5.53	-6.04	-6.50	-3.60	-2.27	0.87	1.39	2.87	2.54	3.72	2.97
	A	**271**	**272**	**273**	**274**	**275**	**276**	**277**	**278**	**279**	**280**	**281**	**282**	**283**	**284**
Z=112	**Qα**	12.07	11.82	11.72	11.61	11.70	12.05	12.30	12.49	12.03	11.34	10.35	9.62	9.22	8.89
	gldm	-5.97	-5.54	-5.34	-5.12	-5.33	-6.05	-6.55	-6.92	-6.06	-4.61	-2.20	-0.16	1.06	2.13
	fit	-4.79	-4.96	-4.07	-4.53	-4.06	-5.53	-5.38	-6.48	-4.85	-4.03	-0.89	0.46	2.36	2.73

Table 2: $Log[T_\alpha(s)]$ for the heaviest elements as functions of the charge and mass of the mother nucleus and Q_α.

118					Q : 12.49 [60, 300] μs T_{fit} : 72 μs T_{gldm} : 3 μs
116				Q : 11.5 [300, 1460] μs T_{fit} : 3000 μs T_{gldm} : 110 μs	
114			Q : 9.55 [290, 1450] μs T_{fit} : 117 s T_{gldm} : 5 s	Q : 9.53 5.5 s T_{fit} : 130 s T_{gldm} : 5.5 s	Q : 9.08 [2, 23] s T_{fit} : 3000 s T_{gldm} : 145 s
112		Q : 10.35 [0.4, 2.2] ms T_{fit} : 130 ms T_{gldm} : 6.3 ms		Q : 8.8 [20, 200] m T_{fit} : 84 m T_{gldm} : 4.5 m	
110	Q : 10.89 [1.5,7.7]ms T_{fit} : 1.3 ms T_{gldm} : 0.07 ms		Q : 8.75(MeV) [1, 12] m T_{fit} : 23 m T_{gldm} : 1.5 m		
Z/N	**167**	**169**	**171**	**173**	**175**

Table 3: Comparison between the experimental α decay half-lives (between square brackets) of the heaviest and superheavy elements [2,3] and the predicted ones by the fitted formulas and the GLDM.

5 Conclusion

The α decay process and particularly the α decay half-lives may be described within a tunneling process below a deformation barrier calculated from a generalized liquid drop model adjusted to reproduce the experimental Q_α value and without introducing a preformation probability factor as for the spontaneous fission. In addition to the GLDM approach, a fitting procedure has also led to accurate formulas for the α decay half-lives. Extrapolations to very heavy and superheavy nuclides have been investigated. The theoretical half-lives are respectively of 5 to 2 orders of magnitude higher than the experimental data for the $^{285}114$ and the $^{289}114$ nuclei apparently observed recently. This perhaps indicate that 114 is not a good magic proton number. The calculated kinetic energy of the fragments is also higher than the apparently measured one.

In the entrance channel, the combination of the generalized liquid drop model and the asymmetric two-center shell model shows that the formation of the nucleon shells before reaching the compound nucleus shape is essential to stabilize the formed nuclear system. The moment of emission of the excess neutrons which evacuate a part of the excitation energy is crucial to decide between complete fusion and fast fission processes.

References

1. S. Hofmann and G. Münzenberg, GSI report 2000-02.
2. V. Ninov et al, *Phys. Rev. Lett.* **83**, 1104 (1999).
3. Y. T. Oganessian et al, *Phys. Rev. Lett.* **83**, 3154 (1999).
4. G. Royer, *J. Phys.* **G,** in press.
5. G. Royer and B. Remaud, *Nucl. Phys.* **A 444**, 477 (1985).
6. G. Royer, Heavy Elements and Related New Phenomena, edited by R. K. Gupta and W. Greiner (World Scientific, 1999) p 591.
7. G. Royer, C. Normand and E. Druet, *Nucl. Phys.* **A 634**, 267 (1998).
8. G. Royer and R. Moustabchir, *Nucl. Phys.* **A,** in press.
9. R. Moustabchir and G. Royer, submitted to Nucl. Phys. **A**.
10. R. A. Gherghescu and G. Royer, *Int. J. Mod. Phys.* **E 9**, 51 (2000).
11. R. Bass, Proc. Conf. on deep inelastic and fusion reactions with heavy ions, Berlin (Springer, 1979) p 281.
12. W. D. Myers and W. J. Swiatecki, *Nucl. Phys.* **A 601**, 141 (1996).
13. P. Armbruster, *E. Phys. J.* **A 7**, 23 (2000).